Shi, Z., Chen, J., and Chen, Q. 2015. "On the turbulence models and turbulent Schmidt number in simulating stratified flows," Accepted by *Journal of Building Performance Simulation*.

On the turbulence models and turbulent Schmidt number in simulating stratified flows

Zhu Shi[a], Jun Chen[a], Qingyan Chen[b,a]
[a] *School of Mechanical Engineering, Purdue University, West Lafayette, IN 47907, USA*
[b] *School of Environmental Science and Engineering, Tianjin University, Tianjin 300072, China*

Jun Chen (Corresponding Author)
Email: junchen@purdue.edu;
Tel.: +1 (765) 494-7050

Abstract

Stratified flows are prevalent in indoor and outdoor environments. To predict these flows, this investigation evaluated the performance of seven turbulence models by comparing the simulation results with the experimental data of both weakly and strongly stratified jets. The models tested included six Reynolds-Averaged Navier-Stokes (RANS) models and one Large Eddy Simulation (LES) model. The velocity, turbulent kinetic energy, and Reynolds stress distributions were examined. For the weakly stratified jet, all seven models could predict well the mean velocity, but for the strongly stratified jet, the RSM and LES models overpredicted the velocity in the unstable stratification region. The SST $k-\omega$ model was the best. This paper also introduced a new dynamic turbulent Schmidt number model which can improve the prediction of density distribution. In addition, this investigation analysed the computing costs of the models as well as the vorticity and entrainment ratios predicted by the models.

Keywords: CFD; turbulent stratified flow; turbulence models; dynamic turbulent Schmidt number model; entrainment

Nomenclature

C_j	Concentration of species j
D	Diameter of jet nozzle, characteristic length scale
D_t	Turbulent eddy diffusivity
g_i	Gravitational acceleration in i direction
G_b	The generation of turbulence kinetic energy due to buoyancy
G_k	The generation of turbulence kinetic energy due to the mean velocity gradients
I	Turbulent intensity
p	Pressure
P_{jk}	Stress production
Re	Reynolds number
Ri	Richardson number
$r_{-1/2}, r_{+1/2}$	The half-width of jet in stable and unstable regions
S_ϕ	Source term of scalar ϕ

Sc_t , $\sigma_{C,t}$	Turbulent Schmidt number
t	Time
u_i	Velocity magnitude in i direction
U_0	Jet initial velocity, characteristic velocity
x_i	Coordinate in i direction
Y_k	Dissipation of k due to turbulence
Y_ω	Dissipation of ω due to turbulence
ρ	Density
ϕ	Scalar component
k	Kinetic energy per unit mass
ε	Turbulent dissipation rate
ω	Specification dissipation rate
$\Gamma_{\phi,eff}$	Coefficient of effective diffusion of scalar ϕ
μ	Dynamic viscosity
μ_t	Turbulent dynamic viscosity
σ_C	Schmidt number
τ_{ij}	Shear stress
Δ	Change in variable
θ	Non-dimensional density difference
ν_t	Turbulent kinematic viscosity
Ω_i	Vorticity in i direction

1 Introduction

Understanding stratified flows that have slightly different densities plays a significant role in indoor aerodynamics (Sørensen and Weschler 2002), environmental and geophysical flow dynamics (Blocken et al. 2007), and other engineering applications. In an indoor environment, for example, an aircraft cabin or building, stratified flow develops when air with different temperatures is supplied into the enclosed space through the HVAC system (Lau 2003). Mixing of fresh water with seawater in the estuary and interaction of warm and cold ocean currents are other examples of stratified flows in nature. In chemical plants, different solutions are mixed, with stratification by different densities or temperatures. Studying the interplay of turbulence and stratification is of keen interest for gaining an understanding of the mixing dynamics needed for optimal design of indoor environments, accurate prediction of geophysical dynamics, and optimal quality of chemical products.

In past years, a variety of experimental studies have been done on stratified flows. Kneller et al. (1999) employed Laser-Doppler Anemometry (LDA) to predict the behavior of stratified gravity currents and obtained two-dimensional information on turbulent flow field and energy distribution. Baines (2001) adopted a particle tracking method to measure the flow

features of dense fluid down gentle slopes into a density-stratified environment and derived a quantitative model to describe turbulent downslope flows into stratified environments. Dalziel et al. (2007) used the synthetic schlieren technique and Particle Image Velocimetry (PIV) to measure the density and velocity fields, respectively, in which the density field measurement was used not only to predict the stratification but also to correct the normal errors related to the refractive index variations in velocity field measurement. Xu and Chen (2012) conducted simultaneous measurements of velocity and density fields in a horizontally introduced stratified jet by combining PIV and Planar Laser-Induced Fluorescence (PLIF) techniques. The measurements revealed the structures of a stratified jet in both stable stratification and unstable stratification regions. The aforementioned experimental studies and similar ones explored various experimental techniques for investigating the structures of stratified flows.

Moreover, with the development of computational resources, computational fluid dynamics (CFD) has become increasingly popular in investigating the fluids problem. Among the different techniques, Reynolds-Averaged Navier-Stokes (RANS) has received the most applications by adopting different turbulent models to close the equations. Two-equation turbulence models have been mainly used in the simulating of stratified flows. Liu et al. (2008) studied the performances of RNG $k-\varepsilon$ model and standard $k-\varepsilon$ model in simulating single-sided natural ventilation driven by stratification effect, which is due to temperature difference. Their comparison with experimental data concluded that RNG $k-\varepsilon$ model performed better than standard $k-\varepsilon$ model in predicting such flow. Ji et al.(2008) adopted the $k-\omega$ model (Wilcox 1988) to investigate naturally ventilated double-skin facades(DSFs) with Venetian blinds inside the facade cavity. The results demonstrated that Venetian blinds could enhance the buoyancy-driven natural ventilation of the facade cavity. Cropper et al. (2010) developed a CFD model to simulate the airflow and temperatures around human body using SST $k-\omega$ model (Menter 1994). This model was further coupled with a thermal comfort model, which was able to predict human thermal comfort in various environmental conditions. Venayagamoorthy et al. (2003) tested the performance of the standard $k-\varepsilon$ model in stably stratified flows, using data from direct numerical simulation (DNS). Their results showed that the buoyancy parameter $C_{\varepsilon 3}$ was a very sensitive parameter for stratified flows. Besides the two-equation models, Spall (1998) adopted the Reynolds Stress Model (RSM), a seven-equation model, to investigate the natural stratification phenomenon in cylindrical thermal storage tanks, showing that the RSM model can give a more accurate prediction of the thermocline thickness than the $k-\varepsilon$ model. These numerical simulations provided detailed information concerning stratified flows, which was complimentary to the experimental results. However, there has still been no systematic evaluation of the performance of different turbulent models at different turbulence and stratification levels, indicated by Reynolds numbers and Richardson numbers, respectively. This is particularly important in the transitional or developing region of the flow since most of the previous studies have been focused on fully-developed regions where many turbulence models have been proven to function well in unstratified flows.

Furthermore, in the simulations of flows with density stratification, a key parameter in predicting density distribution is the turbulent Schmidt number (Sc_t). He et al. (1999) identified the significant effect of the turbulent Schmidt number on the species spreading rate in jet-in-crossflows. The authors also concluded that Sc_t should be a variable in jet-in-crossflows based on a semi-empirical analysis. Tominaga and Stathopoulos (2007) discovered that the optimal

turbulent Schmidt number depended on local flow characteristics and recommended a dynamic determination of Sc_t according to local flow structure. Since Sc_t has a large impact on the species transfer in simulating stratified flows, adopting such a dynamic model is more reasonable than using a constant turbulent Schmidt number in simulating stratified flows, as in most existing practices.

Therefore, there are three-fold objectives in this study: (1) To systematically evaluate the performances of most prevalent models in simulating stratified flows; (2) To further investigate the impact of the turbulent Schmidt number on simulating stratified jets, and to develop a dynamic turbulent Schmidt number model based on local flow structure; (3) To study the entrainment effect and vorticity in stratified jets. This paper reports our effort in the investigation.

2 Research Method

This section describes the most prevalent turbulence models used for predicting stratified jets, the experimental data used for validating the models, the numerical algorithm used in solving the turbulence model, and the dynamic Schmidt number model developed to improve the performance of the turbulence models.

2.1 Turbulence models for stratified flows

Stratified flow with a small density difference can be described by continuity equation

$$\frac{\partial \rho}{\partial t}+\frac{\partial}{\partial x_i}(\rho u_i)=0, \quad \text{(i=1,2,3)} \tag{1}$$

momentum equation

$$\rho \frac{\partial u_j}{\partial t}+\rho u_i \frac{\partial u_j}{\partial x_i}=-\frac{\partial p}{\partial x_j}+\mu \frac{\partial^2 u_j}{\partial x_i \partial x_i}+\rho g_j, \quad \text{(i=1,2,3)} \tag{2}$$

and species (scalar) transport equation

$$\frac{\partial}{\partial t}(\rho C_j)+\rho u_i \frac{\partial C_j}{\partial x_i}=-\frac{\partial J_j}{\partial x_i}, \text{(i=1,2,3)} \tag{3}$$

The details of the modeling for the equations are shown in Table 1.

In a RANS simulation, a specific flow variable is decomposed into mean components and fluctuating components: $u_i=\bar{u}_i+u_i'$, $\phi=\bar{\phi}+\phi'$, where $\bar{u}_i$ and u_i' are the mean and fluctuating velocity components, and $\bar{\phi}$ and ϕ' are the mean and fluctuating scalar components. The mean components are solved from the RANS equations. On the other side, in LES, the flow variables are filtered by a low-pass filtering operation with a chosen filter width (corresponding to the grid spacing used in the computation). As a result, the large eddies are solved from filtered Navier-Stokes equations, and the influence of the unresolved (sub-grid scale, SGS) eddies is described by SGS models.

This investigation used the following prevalent turbulent models: the standard $k-\varepsilon$ model (Launder and Spalding 1972), RNG $k-\varepsilon$ model (Yakhot and Orszag 1986), realizable $k-\varepsilon$ model (Shih, et al. 1994), standard $k-\omega$ model (Wilcox, D.C. 1998), SST $k-\omega$ model (Menter 1994), and RSM model (Gibson and Launder 1978; Launder 1989; Launder and Reece 1975). Since LES has often been believed to yield a more accurate prediction than RANS, LES has also been examined using the Smagorinsky-Lilly model (Smagorinsky 1963). The transport equations for any mean parameter in the turbulence models can be expressed in a general form (White 1991; Patankar 1980):

$$\rho \frac{\partial \bar{\phi}}{\partial t} + \rho \bar{u}_i \frac{\partial \bar{\phi}}{\partial x_i} - \frac{\partial}{\partial x_i}\left[\Gamma_{\phi,eff} \frac{\partial \bar{\phi}}{\partial x_i} \right] = S_\phi \quad (4)$$

where ϕ represents a specific variable, $\Gamma_{\phi,eff}$ the coefficient of effective diffusion, and S_ϕ the source term. Table 1 summarizes the choices of $\Gamma_{\phi,eff}$, S_ϕ and the corresponding constants in the governing equations and turbulence modeling equations used in the current investigation.

2.2 Experimental data of stratified jets

Since the turbulence modeling used approximations, it is essential to validate the computational results using experimental data. The experimental data from a stratified jet (Xu and Chen 2012) were used as benchmarks in the present study to validate and develop the models. Figure 1 shows the schematic of the experiment, and four sets of data were acquired. In two unstratified cases ("high-Re" and "low-Re"), the fluid discharged from the jet nozzle had the same density as the fluid in the tank. In two stratified cases ("high-Ri" and "low-Ri"), the fluid injected into the tank was of higher density than the fluid in the tank, leading to density stratification. In order to quantify the degree of stratification, the Richardson number was employed: $Ri_0 = \Delta\rho_0 Dg/(\rho U_0^2)$, where $\Delta\rho_0$, D, U_0 are the characteristic density differences, length scale, and velocity, respectively. In the experiment, both velocity and density fields were measured with the combined PIV and PLIF system. With the velocity and density data, Xu and Chen examined averaged parameters, Reynolds stresses, vertical density flux, turbulent kinetic energy budget, etc., within central vertical plane. Although measurements were available in both the unstratified and stratified cases, the current investigation mainly focuses on the numerical calculations in stratified cases. The details of "high-Ri" and "low-Ri" cases were summarized in Table 2. Average velocity, average density, turbulent kinetic energy and Reynolds stress values were examined in the present study.

In this horizontal stratified jet, both stable and unstable stratification regions exist, as shown in Fig. 1. Stable stratification was formed where $d\bar{\rho}/dz > 0$ and turbulence were weakened by the buoyancy effect. Unstable stratification was formed where $d\bar{\rho}/dz < 0$ and turbulence was enhanced by the buoyancy effect. The measurements enable comparative studies in both stable and unstable stratification regions.

2.3 Numerical simulations of the stratified jets

Our numerical simulation of the stratified jet flow used the following assumptions: (1) Since the averaged flow field was symmetric with respect to the central vertical plane (y=0), half of the domain was used in the RANS simulations. In LES, the whole domain should be used to resolve the three dimensional unsteady flow motions. (2) A solid cylinder was deployed in the tank to simulate the existence of the jet nozzle, and the velocity and scalar profiles at the jet exit were prescribed as boundary conditions. Fig. 2a shows the dimensions of the computation domain, which is exactly the same size as in the experiment. Fig. 2b, 2c and 2d present the mesh of the CFD model for RANS cases. The mesh structure for LES simulation was very similar to that shown in Fig. 2, but the grids were much finer, as detailed below.

This study adopted a non-uniform grid size method for the meshing. The grid was the finest at the jet nozzle and gradually increased from the nozzle. To check grid independence, RANS simulations (using the standard $k-\varepsilon$ model) of the Low-Ri case were conducted on three different grids: 214,990, 431,280, and 811,190 grids, respectively, representing coarse, medium, and fine grids. However, different numbers of cells were used on the jet axes and cross-

sections (vertical to axes) of the fluid domain. The table in Fig. 3 describes the detailed differences of the three grids. Fig. 3 also shows the velocity profiles along the centerline from these three grid systems. The results from the coarse and medium grids showed significant differences, while the results from the medium and fine grids almost collapsed. This suggests that the medium grid led to grid-independent results and the grid was used in the following RANS simulations. Since LES needs to use the entire domain and it typically requires finer meshes, the grid independence test for LES was conducted separately in a similar way. The number of grids for LES was finalized at 1,624,130.

This study employed a numerical solver in ANSYS Fluent 14.0 to solve equations (1) to (3) to obtain the flow and scalar fields. Pressure-velocity was coupled using the SIMPLE scheme. The second-order upwind scheme was used to discretize the momentum, turbulent kinetic energy, and species term. In order to assure accuracy, the second order implicit method was employed for the transient formulation. Unsteady simulations were adopted with time step 0.005s. A sensitivity study was also done on time step size by confirming that a smaller time step did not change the simulation results a lot. At each time step, 30 iterations were conducted. Within each time step, x, y and z velocity residuals dropped by 4 orders of magnitude; at the end of each time step size, energy residual decreased to 10^{-8}, and scaled species residual decreased to 10^{-7}. For LES simulations, 3-second time interval was used for data collecting and averaging in obtaining averaged values from instantaneous parameters.

At the jet exit, the velocity and scalar (mass fraction) profiles were prescribed according to the experimental data. The right boundary of the calculation domain was defined as a pressure-outlet, which served as an outlet for the flow. (For the pressure-outlet boundary, when gravity was enabled in the calculation, the increase of pressure due to gravity was considered automatically.) In the experiment, the topside was the interface between the fluid and the atmosphere, so the zero-shear (symmetry) boundary condition was defined for the top boundary in the present simulation. For other boundaries, no-slip boundary conditions were specified.

2.4 Dynamic Schmidt number model

To simulate the stratified flows using eddy-viscosity-type models, the vertical momentum flux and density flux along the buoyancy direction were two key parameters being modeled by eddy viscosity ν_t and eddy diffusivity D_t:

$$\overline{u_1' u_3'} = -\nu_t \frac{\partial \overline{u}_1}{\partial x_3} \quad \text{and} \quad \overline{\theta' u_3'} = -D_t \frac{\partial \overline{\theta}}{\partial x_3} \tag{5}$$

In particular, ν_t and D_t were related to turbulent Schmidt number $Sc_t = \nu_t / D_t$, which is usually chosen as a constant. Many aforementioned studies have shown the deficiency of such a simple model. For example, Xu and Chen (2012) demonstrated that density flux ($\overline{\theta' u_3'}$) was not only dependent on density gradient, but also on velocity gradient. The present study proposed a dynamic turbulent Schmidt number model that relates the local Sc_t with a local velocity gradient and scalar gradient. If one assumes in stratified flows that momentum flux and density flux are dependent on velocity gradient and density gradient and applies the Taylor expansion, i.e.,

$$\overline{u_1'u_3'} = f\left(\frac{\partial\overline{u}_1}{\partial x_3}, \frac{\partial\overline{\theta}}{\partial x_3}\right) = A_1\frac{\partial\overline{u}_1}{\partial x_3} + A_2\left(\frac{\partial\overline{u}_1}{\partial x_3}\right)^2 + \cdots + B_1\frac{\partial\overline{\theta}}{\partial x_3} + B_2\left(\frac{\partial\overline{\theta}}{\partial x_3}\right)^2 + \cdots \quad (6)$$

$$\overline{\theta' u_3'} = g\left(\frac{\partial\overline{u}_1}{\partial x_3}, \frac{\partial\overline{\theta}}{\partial x_3}\right) = C_1\frac{\partial\overline{u}_1}{\partial x_3} + C_2\left(\frac{\partial\overline{u}_1}{\partial x_3}\right)^2 + \cdots + D_1\frac{\partial\overline{\theta}}{\partial x_3} + D_2\left(\frac{\partial\overline{\theta}}{\partial x_3}\right)^2 + \cdots \quad (7)$$

where the A_i, B_i, C_i, and D_i were expansion coefficients (i=1, 2). When the first-order approximation was employed,

$$\overline{u_1'u_3'} \approx A_1\frac{\partial\overline{u}_1}{\partial x_3} + B_1\frac{\partial\overline{\theta}}{\partial x_3} \quad \text{and} \quad \overline{\theta' u_3'} \approx C_1\frac{\partial\overline{u}_1}{\partial x_3} + D_1\frac{\partial\overline{\theta}}{\partial x_3} \quad (8)$$

Then the expression of Sc_t led to

$$Sc_t = \frac{\nu_t}{D_t} = \frac{\left(A_1\frac{\partial\overline{u}_1}{\partial x_3} + B_1\frac{\partial\overline{\theta}}{\partial x_3}\right)/\frac{\partial\overline{u}_1}{\partial x_3}}{\left(C_1\frac{\partial\overline{u}_1}{\partial x_3} + D_1\frac{\partial\overline{\theta}}{\partial x_3}\right)/\frac{\partial\overline{\theta}}{\partial x_3}} = \frac{A_1 + \frac{B_1}{\frac{\partial\overline{u}_1}{\partial x_3}/\frac{\partial\overline{\theta}}{\partial x_3}}}{D_1 + C_1\frac{\partial\overline{u}_1}{\partial x_3}/\frac{\partial\overline{\theta}}{\partial x_3}} \quad (9)$$

Sc_t thus can be expressed as a function of $\frac{\partial\overline{u}_1}{\partial x_3}/\frac{\partial\overline{\theta}}{\partial x_3}$, or its normalized term $\frac{\partial\overline{u}_1^*}{\partial x_3^*}/\frac{\partial\overline{\theta}}{\partial x_3^*}$(

$x_3^* = \frac{x_3}{D}, \overline{u}_1^* = \frac{\overline{u}_1}{U_0}$, where D and U_0 are the characteristic length scale and characteristic velocity.

By using Taylor's expansion again and denoting $t = \frac{\partial\overline{u}_1^*}{\partial x_3^*}/\frac{\partial\overline{\theta}}{\partial x_3^*}$, Sc_t can be expressed as

$$Sc_t = h(t) = \alpha_0 + \alpha_1 t + \alpha_2 t^2 + \cdots \quad (10)$$

where the model coefficients α_i's can be determined by the experimental data, as shown in Fig. 4, for both high-Ri and low-Ri cases, as well as different downstream locations.

The fitting yielded two coefficients: α_0=1.57 and α_1=-0.46, where the higher order terms were neglected. Thus, the turbulent Schmidt number can be dynamically expressed as:

$$Sc_t = 1.57 - 0.46t \quad (11)$$

In the present study, this dynamic turbulent Schmidt number model (DTSN-Model) is applied when the velocity gradient and scalar gradient fall into the following range: $|\partial(\overline{u}_1/U_0)/\partial(x_3/D)| > 0.005$, the region where most mixing processes happened and where the experimental Sc_t values were selected for DTSN-model development. The model was implemented into the RANS models through a user-defined function.

3 Results

Fig. 5 shows the velocity contours and streamlines for both weak stratification (low-Ri) and strong stratification (high-Ri) cases. The present study evaluates the performance of six RANS models and LES in stratified flow, under the two cases. For each case, first order moment (mean

velocity) and second order moments (turbulent kinetic energy and Reynolds stresses) were compared with experimental data at fully-developed downstream locations (x=20D for low-Ri case and x=10D for high-Ri case, respectively). The turbulent kinetic energy is

$$TKE = \frac{1}{2}\left(\overline{u_1'u_1'} + \overline{u_2'u_2'} + \overline{u_3'u_3'}\right) \tag{12}$$

and a shear Reynolds stress, $\overline{u_1'u_3'}$, were compared with the experimental data.

As suggested by Britter and Schatzmann (2007), quantitative comparison with experimental data is a good method to evaluate the performances of various turbulence models. Thus MSE (Mean Squared Error) (Lehmann and Casella 1998) was used to describe the degree of deviation of predicted values from experimental values in this study. MSE is defined as

$$MSE = \frac{1}{N}\sum_{i=1}^{N}(X_{p,i} - X_{m,i})^2, \tag{13}$$

where $X_{p,i}$ is the predicted value at i-th location, $X_{m,i}$ is the measured value at i-th location and N is the number of locations compared.

Furthermore, the proposed DTSN-model was tested by investigating the predicted scalar distribution.

3.1 Mean velocity

In the horizontally introduced stratified jet, its centerline deviates from the horizontal direction due to the buoyancy effect, as demonstrated in Fig. 6. To quantify the degree of this deviation, z_c was defined such that $U_c(x) = \bar{u}_1(x, 0, z_c)$, where $U_c(x)$ was the peak value at downstream location x. Meanwhile, to characterize the jet expansion, two half-width locations, $z_{+1/2}$ and $z_{-1/2}$ were defined in stable and unstable regions, respectively:

$$\bar{u}(x, 0, z_{+1/2}) = \bar{u}(x, 0, z_{-1/2}) = U_c/2 \tag{14}$$

The corresponding half-widths of the jet in stable and unstable regions were defined respectively:

$$r_{-1/2} = z_c - z_{-1/2}\ ,\ r_{+1/2} = z_{+1/2} - z_c \tag{15}$$

The self-similarity characteristics of a homogenous round jet, $\bar{u}/U_c$ vs. $r/r_{1/2}$, can be found in many other studies, e.g., Pope (2001).

Fig. 7 shows the self-similarity curves from the experimental data and simulation results. Due to the stratification, z coordinate was normalized as $(z - z_c)/r_{1/2}$, where $r_{1/2} = (r_{-1/2} + r_{+1/2})/2$. In the low-Ri case (Fig. 7a), the simulation results agree well with the experimental data in the stable stratification region, but in the unstable stratification region, a discrepancy was observed for certain turbulence models. Based on the MSE values from Table 3, the SST $k-\omega$ model, standard $k-\varepsilon$ model and RNG $k-\varepsilon$ model yielded the best performances, while the results from the other models were still acceptable. This shows that when the stratification was weak and the turbulence effect was dominant (Re=24,000), these models could yield an accurate prediction of the mean velocity.

In the high-Ri case (Fig. 7b), the stratified jet bends more quickly than in the low-Ri case. Overall, the performances of the turbulence models were worse in the high-Ri case than in the low-Ri case. This indicates that most of the tested models work better in high Reynolds number flows than in low or transitional Reynolds number flows. The prediction accuracy in the stable

stratification region was different from the one in the unstable stratification region. In the stable stratification region, all the turbulence models gave acceptable predictions of the mean velocity. However, in the unstable stratification region, large discrepancies from the experimental results were observed in the results from the RSM model and LES. Although the RSM model solved transport equations for Reynolds stresses, which can be helpful for predicting second order flow characteristics, it was deficient in predicting the mean velocity when the stratification was strong. The LES result in the unstable stratification region deviated even more from the experimental data than the RSM result, possibly due to the problem of the Smogrinsky-Lilly model for flow in a transitional region. As indicated by Voke (1996), the coefficients of the Smagorinsky-Lilly model are proportional to the square of the grid scale, and vanish too slowly when the Reynolds number is low. As a result, LES with the Smagorinsky-Lilly model overpredicts the subgrid eddy-viscosity. Our results show once again that the prediction of flow features in the unstable stratification region was more difficult than in the stable stratification region. The MSE values showed that SST $k-\omega$ model gave the best mean velocity profile among all the models tested, similar to the tests for the low-Ri case. One important advantage of the SST $k-\omega$ model is that a low Reynolds number correction can be used to damp the turbulent viscosity in low Reynolds number simulations.

3.2 Turbulent kinetic energy

Fig. 8 shows the predicted TKE at a downstream location in low-Ri and high-Ri cases, and Table 4 illustrates the MSE values under various models. For the low-Ri case (Fig. 8a), among all the two-equation models, the SST $k-\omega$ model led to the best results. The three variations of $k-\varepsilon$ models also captured the general trend of the TKE profile. However, standard $k-\omega$ significantly underpredicted TKE at the core region of the jet (-2<z/D<2). Compared to the standard $k-\omega$ model, the SST $k-\omega$ model modified the turbulent viscosity formulation to account for the transport effects of the principal turbulent shear stress. Since the stratified jet flow was a typical shear stress flow, that is why the SST $k-\omega$ model yielded a significantly better prediction. The RSM model also led to acceptable prediction of TKE. The experimental result shows a "dent" around the center of the jet, and the RSM was the only model that could predict it. On the other hand, LES did not produce satisfactory results as expected because the SGS model tested in the present study may be the source of the prediction error.

Fig. 8b compares the TKE profiles predicted with the experimental data in the high-Ri case. Due to the strong stratification in the high-Ri case, the TKE profile was asymmetric and the peak deviated downwards. Similar to in the low-Ri case, the RSM and SST $k-\omega$ models gave good predictions of the TKE distribution at locations close to jet axis, and SST $k-\omega$ model gave the best overall TKE predictions. LES overpredicted significantly the TKE, which may be attributed to the deficiency of the Smagorinsky-Lilly model in low Reynolds number flows. Overall, the predictions of TKE in this case were not as accurate as those in the low-Ri case, which was similar for the mean velocity.

3.3 Shear stress

Figure 9 shows the comparison between shear stresses. From Table 5, for the low-Ri case, the models that performed well in predicting TKE, the SST $k-\omega$ model, and the RSM model, also gave good predictions of $\overline{u_1'u_3'}$, especially in stable stratification region. The RSM model solves the transport equation for Reynolds stresses, while other eddy viscosity models relies on the assumption that μ_t was isotropic, which is not true in stratified flows. Thus, the RSM model was better in predicting Reynolds stresses than mean velocities. Since the RNG $k-\varepsilon$ model can take

the stratification effects (Moghaddasi-Naini et al. 1998) into account, it also performed well. For shear stress results, all predicted profiles captured the inverse-symmetric characteristic. However, the magnitude in the unstable stratification region was underpredicted compared with in the stable stratification region. This indicates that the simulations in the unstable stratification region were more difficult due to the complex physics of fluid in this region.

For the high-Ri case, the RNG $k-\varepsilon$ model still yielded the best prediction among all three $k-\varepsilon$ models, although its prediction performance in the unstable region was much worse than in the stable region. The SST $k-\omega$ model and RSM model also underpredicted the shear stress in the unstable stratification regions. However, these two models performed best when evaluated by the overall results. All the other RANS models underpredicted the stresses. LES overpredicted the shear stress in stable stratification region but underpredicted it in unstable stratification region.

3.4 Predictions of scalar distribution

Section 5 introduced a new dynamic turbulent Schmidt number model. By applying it to the SST $k-\omega$ model that gave the best prediction of the mean flow characteristics above, this investigation could evaluate the impact of the turbulent Schmidt number in predicting a scalar, dimensionless density difference $\theta=(\rho-\rho_{ambient})/\Delta\rho$. The "standard" turbulent Schmidt number has been controversial (He et al. 1999; Tominaga et al. 2007). He et al. (1999) suggested $Sc_t=0.2$ for a jet-in-cross flow, which is very similar to the stratified jet in this study. A constant turbulent Schmidt number 0.7 is always recommended in commercial CFD software as the default value. The present investigation evaluates the difference in choosing three turbulent Schmidt numbers: $Sc_t=0.2$, $Sc_t=0.7$, and Sc_t determined by DTSN (equation 12).

Fig. 10 and Fig. 11 show normalized density distributions at two different locations (between x=10D and x=20D, indicated by "upstream" and "downstream," respectively) in both the low-Ri and high-Ri cases. The predicted density difference distributions in the stratified flows were highly dependent on the turbulent Schmidt number. The variable DTSN-model gave the best density distributions, especially in downstreams. One may also note that the larger the value of Sc_t was, the higher the predicted peak density was. This is because the mixing of the two species in the stratified flows was inversely dependent on Sc_t. A lower Sc_t can diffuse dense fluid faster into the ambient light fluid, and thus, lead to a lower peak density.

3.5 Prediction of vorticity in the stratified jets

Studying vorticity is important for characterizing the local flow structure. Fig. 12 shows the vorticy contours at the center vertical plane in the low-Ri and high-Ri cases predicted by the SST $k-\omega$ model and compares them to the experimental data. In the low-Ri case, the vorticity distribution was almost antimetric, and the boundary between negative and positive vorticity was basically the centerline when x/D<15. In the high-Ri case, in contrast, the boundary bent downwards with the increase of x/D. The vorticity in the stable stratification region was larger than in the unstable stratification region. Overall, the vorticity distributions in both the weak and strong stratification jets were captured with acceptable accuracy. These results show again that the SST $k-\omega$ model can predict the stratified flow characteristics.

3.6 Entrainments in the stratified jets

The numerical simulations also enable us to analyze the entrainment in the stratified jets. The

entrainment ratio is defined as $\frac{m}{m_0}$, where m_0 is the mass of fluid discharged from the jet nozzle and m is the mass across a section perpendicular to the jet. Ricou and Spalding (1960) concluded that the entrainment ratio of a horizontal jet could be expressed by using an empirical formula: $\frac{m}{m_0} = 0.32(\frac{\rho_1}{\rho_0})^{\frac{1}{2}} \frac{x}{D}$, where ρ_0 is the density of the fluid discharged from the nozzle, and ρ_1 is the density of ambient fluid. In this study, we employed the SST $k-\omega$ model to predict the entrainment ratio and compared the results with those of the empirical formula.

As shown in Fig. 13, both methods gave a good prediction for the entrainment ratio when x/D<30, where the increase of the entrainment ratio was proportitional to x/D. However, a large discrepancy was found where x/D>30. This was mainly due to the confinement of the fluid tank, which decreased the amount of entrainment. The empirical formula assumed a perfect free-jet. Due to the entrainment, the percentage of fluid in the jet from the nozzle (called "new fluid") decreased as x/D increased. When x/D>30, only about 10% of the fluid in the jet originated from the nozzle.

The entrainment in the high-Ri case was much more complex than in the low-Ri case. The entrainment ratio predicted by the SST $k-\omega$ model was smaller than that from the empirical formula. The reason is that the strong buoyancy effect in the high-Ri jet bent the jet heavily, which led to a decrease in the entrainment while the empirical formula assumed the buoyancy effect to be negligible. Therefore, the empirical formula should not be used for determining the jet entrainment with strong stratification. The numerical prediction in Fig. 14 shows that the entrainment ratio curve can be divided into a linear region and a nonlinear region. In the linear region, the entrainment ratio increased with x/D with a linear coefficient of 0.235, a much smaller value than 0.32 in the empirical formula. The entrainment ratio in the nonlinear region increased more slowly than in the linear region due to the impingement of the jet at the tank wall, which decreased the entrainment amount.

4 Discussions on computation costs

This study also evaluated the computation time by these seven models. All the six RANS models used the grid number of 431,280. Due to the high requirement for the grid resolution, the LES simulation used a much larger grid number of 1,624,130, which is about four times that for RANS simulations. The high-Ri case was used for comparison. All the simulations were tested on one node of a Linux-cluster with two 2.5 GHz Quad-Core AMD 2380 processors.

The calculation time for running a 12-second interval transient simultion with different models was recorded and plotted in Fig. 15. Among all the $k-\varepsilon$ models, the RNG $k-\varepsilon$ model required the longest computation time. The computation cost of the SST $k-\omega$ model was slightly higher than that of the standard $k-\omega$ model. Nevertheless, the computation costs of all five eddy-viscosity models were close. The computation cost of the RSM models was about 25% higher than the average of the eddy-viscosity models. This is understandable because the RSM model solved seven transport equations for turbulence parameters, while the eddy-viscosity model solved only two for turbulence. The LES simulation required about twice as much computation time as the RSM and almost three times the average computation time for the eddy-viscosity models. This is mainly attributed to the much larger number of grids used in the LES than in the RANS simulations. Note that the use of DTSN requires 10% additional computation time for calculating the dynamic Schmidt number.

5 Conclusion

The investigation led to the following conclusions:

(1) This investigation evaluated the performances of six RANS models and one LES model in predicting stratified flows. In the weakly stratified flow where the turbulent effect was dominant, all seven models could predict accurately the mean flow, but with large discrepancies in predicting the second-order flow characteristics. Overall, the RNG $k-\varepsilon$ and SST $k-\omega$ models performed very well, but the SST $k-\omega$ was the best. The superiority of LES was not observed in predicting the second-order flow characteristics.

(2) It was more difficult for the models to predict strongly stratified flow. All the models could still predict well the mean flow in the stable stratification region, but the RSM model and LES overestimated the velocity in the unstable stratification region. For predicting the second-order flow characteristics, the RSM, SST $k-\omega$ and RNG $k-\varepsilon$ models can be used, and the first two yielded the best overall results. The LES with the standard Smagorinksy model may not be suitable for the low Reynolds number transitional flows in this study. Therefore, LES does not always give better predicting results than RANS models, although it usually takes much longer time.

(3) This current paper shows that turbulent Schmidt number has large impact on scalar distribution prediction. Thus attention should be paid to it in scalar filed simulation. This study proposed a new dynamic turbulent Schmidt number model based on local velocity gradient and density gradient. The model can improve simulating scalar variables, such as density difference distributions in the jets.

(4) The computation costs of the five eddy-viscosity models in RANS were comparable, but the RSM model required 25% more computing time, and the LES needed three times more computing time. The adoption of the dynamic turbulent Schmidt number model used an additional 10% computing time.

(5) The CFD models can predict vorticity distributions in the stratified jets. The entrainment ratio can be calculated by the empirical formula for the weakly stratified jet but not for the strongly stratified jet. It is not suggested to use empirical formula to predict entrainment ratio when stratification is strong in jet flows.

References

ANSYS. Inc. 2011. ANSYS Fluent Theory Guide, release 14.0 [online]. Available from http://www.ansys.com [Accessed 12 November 2012]

Bacon, S. 1998. "Decadal variability in the outflow from the Nordic seas to the deep Atlantic Ocean." *Nature* 394 (6696): 871-874.

Blocken, B., T. Stathopoulos, and J. Carmeliet. 2007. "CFD simulation of the atmospheric boundary layer: wall function problems." *Atmospheric environment* 41 (2): 238-252.

Britter, R., and M. Schatzmann. (Ed.). 2007. "Background and justification document to support the model evaluation guidance and protocol: COST action 732 Quality assurance and improvement of microscale meteorological models." Hamburg: University of Hamburg Meteorological Institute.

Cropper, P. C., T. Yang, M. Cook, D. Fiala, and R. Yousaf. 2010. "Coupling a model of human thermoregulation with computational fluid dynamics for predicting human–environment interaction." *Journal of Building Performance Simulation* 3 (3): 233-243.

Dalziel, S. B., M. Carr, J. K. Sveen, and P. A. Davies. 2007. "Simultaneous synthetic schlieren and PIV measurements for internal solitary waves." *Measurement Science and Technology* 18 (3): 533.

Ghaisas, N. S., D. A. Shetty, and S. H. Frankel. 2013. "Large eddy simulation of thermal driven cavity: Evaluation of sub-grid scale models and flow physics." *International Journal of Heat and Mass Transfer* 56 (1): 606-624.
Gibson, M. M., and B. E. Launder. 1978. "Ground effects on pressure fluctuations in the atmospheric boundary layer." *Journal of Fluid Mechanics* 86 (03): 491-511.
He, G., Y. Guo, and A. T. Hsu. 1999. "The effect of Schmidt number on turbulent scalar mixing in a jet-in-crossflow." *International Journal of Heat and Mass Transfer* 42 (20): 3727-3738.
Hill, B. J. 1972. "Measurement of local entrainment rate in the initial region of axisymmetric turbulent air jets." *Journal of Fluid Mechanics* 51 (04): 773-779.
Ji, Y., M. J. Cook, V. Hanby, D. G. Infield, D. L. Loveday, and L. Mei. 2008. "CFD modelling of naturally ventilated double-skin facades with Venetian blinds." *Journal of Building Performance Simulation* 1 (3): 185-196.
Kneller, B. C., S. J. Bennett, and W. D. McCaffrey. 1999. "Velocity structure, turbulence and fluid stresses in experimental gravity currents." *Journal of Geophysical Research: Oceans (1978–2012)* 104 (C3): 5381-5391.
Lau, J., and J. L. Niu. 2003. "Measurement and CFD simulation of the temperature stratification in an atrium using a floor level air supply method." *Indoor and Built Environment* 12 (4): 265-280.
Launder, B. E., G. Jr Reece, and W. Rodi. 1975. "Progress in the development of a Reynolds-stress turbulence closure." *Journal of Fluid Mechanics* 68 (03): 537-566.
Launder, B. E. 1989. "Second-moment closure: present… and future?." *International Journal of Heat and fluid flow* 10 (4): 282-300.
Launder, B. E., and D. B. Spalding. 1972. "Lectures in mathematical models of turbulence." London: Academic press.
Lehmann, E. L., and G. Casella. 1998. *Theory of point estimation.*Vol. 31. Berlin: Springer.
Liu, X., J. Niu, M. Perino, and P. Heiselberg. 2008. "Numerical simulation of inter-flat air cross-contamination under the condition of single-sided natural ventilation." *Journal of Building Performance Simulation* 1 (2): 133-147.
Menter, F. R., M. Kuntz, and R. Langtry. 2003. "Ten years of industrial experience with the SST turbulence model." *Turbulence, Heat and Mass transfer* 4: 625-632.
Menter, F. R. 1994. "Two-equation eddy-viscosity turbulence models for engineering applications." *AIAA Journal* 32 (8): 1598-1605.
Moghaddasi-Naini, H.R., S. W. Armfield, and J. Reizes. 1998. "Simulation of stratified flow around a square cylinder using the RNG k-epsilon turbulence model." *In: Proceedings of the 13th Australian Fluid Mechanics Conference*, Melbourne, Australia.
Orszag, S. A., V. Yakhot, W. S. Flannery, F. Boysan, D. Choudhury, J. Maruzewski, and B. Patel. 1993. "Renormalization group modeling and turbulence simulations." *Near-wall Turbulent Flows*: 1031-1046.
Pope, S. B. 2000. *Turbulent Flows*. Cambridge: Cambridge university press.
Ricou, F. P., and D. B. Spalding. 1961. "Measurements of entrainment by axisymmetrical turbulent jets." *Journal of Fluid Mechanics* 11 (01): 21-32.
Shih, T-H., W. W. Liou, A. Shabbir, Z. Yang, and J. Zhu. 1994. "A new k-epsilon eddy viscosity model for high Reynolds number turbulent flows: Model development and validation." *NASA STI/Recon Technical Report* N 95: 11442.
Smagorinsky, J. 1963. "General circulation experiments with the primitive equations: I. The basic experiment*." *Monthly Weather Review* 91 (3): 99-164.

Sørensen, D. N., and C. J. Weschler. 2002. "Modeling-gas phase reactions in indoor environments using computational fluid dynamics." *Atmospheric Environment* 36 (1): 9-18.
Spall, R. E. 1998. "A numerical study of transient mixed convection in cylindrical thermal storage tanks." *International Journal of Heat and Mass Transfer* 41 (13): 2003-2011.
Tominaga, Y., and T. Stathopoulos. 2007. "Turbulent Schmidt numbers for CFD analysis with various types of flowfield." *Atmospheric Environment* 41 (37): 8091-8099.
Venayagamoorthy, S. K., J. R. Koseff, J. H. Ferziger, and L. H. Shih. 2003. "Testing of RANS turbulence models for stratified flows based on DNS data. " Stanford: Stanford University environmental fluid mechanics laboratory.
Voke, P. R. 1996. "Subgrid-scale modelling at low mesh Reynolds number." *Theoretical and Computational Fluid Dynamics* 8 (2): 131-143.
Wilcox, D. C. 1988. "Multiscale model for turbulent flows." *AIAA Journal* 26 (11): 1311-1320.
Wilcox, D. C. 1998. *Turbulence modeling for CFD.* Vol. 2. La Canada, CA: DCW industries.
Xu, D., and J. Chen. 2012. "Experimental study of stratified jet by simultaneous measurements of velocity and density fields*." Experiments in Fluids* 53 (1): 145-162.
Yakhot, V., and S. A. Orszag. 1986. "Renormalization group analysis of turbulence. I. Basic theory." *Journal of Scientific Computing* 1 (1): 3-51.

Table 1. Coefficients of Equation (4)

Equation or model		ϕ	$\Gamma_{\phi,eff}$	S_ϕ	Constants
Reynolds averaged variables	Continuity	1	0		
	Momentum	u_j	$\mu+\mu_t$	$-\frac{\partial p}{\partial x_i}+\frac{\partial}{\partial x_j}\left[(\mu+\mu_t)\frac{\partial u_j}{\partial x_i}\right]$	
	Species	C	$\mu/\sigma_C+\mu_t/\sigma_{C,t}$	S_C	$\sigma_{C,t}$: turbulent Schmidt number
2-equation	(1) Standard $k-\varepsilon$	k	$\mu+\mu_t/\sigma_k$	$G_k+G_b-\rho\varepsilon$	$\mu_t=\rho C_\mu\frac{k^2}{\varepsilon}$, $G_k=\mu_t S^2$, $S=\sqrt{2S_{ij}S_{ij}}$, $G_b=\beta g_i\frac{\partial\mu_t}{\partial\sigma_{T,t}}\frac{\partial\overline{T}}{\partial x_i}$, $C_{1\varepsilon}=1.44$, $C_{2\varepsilon}=1.92$, $C_\mu=0.09$, $\sigma_k=1.0$, $\sigma_\varepsilon=1.3$
		ε	$\mu+\mu_t/\sigma_\varepsilon$	$C_{1\varepsilon}G_k\frac{\varepsilon}{k}-C_{2\varepsilon}\rho\frac{\varepsilon^2}{k}$	
	(2) Realizable $k-\varepsilon$	k	$\mu+\mu_t/\sigma_k$	$G_k+G_b-\rho\varepsilon$	$\mu_t=\rho C_\mu\frac{k^2}{\varepsilon}$, $G_k=\mu_t S^2$, $S=\sqrt{2S_{ij}S_{ij}}$, $G_b=\beta g_i\frac{\partial\mu_t}{\partial\sigma_{T,t}}\frac{\partial\overline{T}}{\partial x_i}$, $C_1=\max\left[0.43,\frac{\eta}{\eta+5}\right]$, $\eta=S\frac{k}{\varepsilon}$, $C_\mu=\frac{1}{A_0+A_s\frac{kU^*}{\varepsilon}}$, $U^*\equiv\sqrt{S_{ij}S_{ij}+\tilde{\Omega}_{ij}\tilde{\Omega}_{ij}}$, $C_{1\varepsilon}=1.44$, $C_2=1.9$, $\sigma_k=1.0$, $\sigma_\varepsilon=1.2$
		ε	$\mu+\mu_t/\sigma_\varepsilon$	$\rho C_1 S\varepsilon-\rho C_2\frac{\varepsilon^2}{k+\sqrt{\upsilon\varepsilon}}$	
	(3) RNG $k-\varepsilon$	k	$\mu+\mu_t/\sigma_k$	$G_k+G_b-\rho\varepsilon$	$\mu_t=\rho C_\mu\frac{k^2}{\varepsilon}$, $G_k=\mu_t S^2$, $S=\sqrt{2S_{ij}S_{ij}}$, $G_b=\beta g_i\frac{\partial\mu_t}{\partial\sigma_{T,t}}\frac{\partial\overline{T}}{\partial x_i}$,

		ε	$\mu+\mu_t/\sigma_\varepsilon$	$C_{1\varepsilon}G_k\frac{\varepsilon}{k}-C_{2\varepsilon}\rho\frac{\varepsilon^2}{k}-R_\varepsilon$	$R_\varepsilon=\frac{C_\mu\rho\eta^3(1-\eta/\eta_0)}{1+\beta\eta^3}\frac{\varepsilon^2}{k}$, $\eta\equiv Sk/\varepsilon$, $\eta_0=4.38$, $\beta=0.012$, $C_{1,\varepsilon}=1.42$, $C_{2,\varepsilon}=1.68$, $C_\mu=0.0845$, $\sigma_k=1.0$, $\sigma_\varepsilon=1.3$
	(4) Standard $k-\omega$	k	$\mu+\mu_t/\sigma_k$	G_k-Y_k	$\mu_t=\alpha^*\frac{\rho k}{\omega}$, $\alpha^*=\begin{cases}High-\mathrm{Re}:\alpha^*_\infty=1\\ Low-\mathrm{Re}:\alpha^*_\infty\left(\frac{\alpha^*_0+\mathrm{Re}_t/R_k}{1+\mathrm{Re}_t/R_k}\right)\end{cases}$, $\mathrm{Re}_t=\frac{\rho k}{\mu\omega}$, $R_k=6$, $\alpha^*_0=\frac{\beta_i}{3}$ $\beta_i=0.072$, $G_k=\mu_t S^2$, $G_\omega=\alpha\frac{\omega}{k}G_k$, $Y_k=\rho\beta^* f_{\beta^*}k\omega$, $Y_\omega=\rho\beta f_\beta\omega^2$, $\beta^*_\infty=0.09$, $\sigma_k=2.0$, $\sigma_\omega=2.0$
		ω	$\mu+\mu_t/\sigma_\omega$	$G_\omega-Y_\omega$	
	(5) SST $k-\omega$	k	$\mu+\mu_t/\sigma_k$	G_k-Y_k	$\mu_t=\frac{\rho k}{\omega}\frac{1}{\max\left[\frac{1}{\alpha^*},\frac{SF_2}{a_1\omega}\right]}$, $\sigma_k=\frac{1}{F_1/\sigma_{k,1}+(1-F_1)/\sigma_{k,2}}$, $\sigma_\omega=\frac{1}{F_1/\sigma_{\omega,1}+(1-F_1)/\sigma_{\omega,2}}$, $G_k=\mu_t S^2$, $G_\omega=\frac{\alpha}{\nu_t}\tilde{G}_k$, $\tilde{G}_k=\min(G_k,10\rho\beta^*k\omega)$, $Y_k=\rho\beta^*k\omega$, $Y_\omega=\rho\beta\omega^2$, $\sigma_{k,1}=1.176$, $\sigma_{\omega,1}=2.0$, $\sigma_{k,2}=1.0$, $\sigma_{\omega,2}=1.168$, $a_1=0.31$
		ω	$\mu+\mu_t/\sigma_\omega$	$G_\omega-Y_\omega$	
7-equation	(6) RSM	$\overline{u'_j u'_k}$	$\mu+\mu_t/\sigma_i$	$P_{jk}+G_{jk}+\phi_{jk}-\varepsilon_{jk}$	$P_{jk}=-\rho\left(\overline{u'_j u'_i}\frac{\partial u_k}{\partial x_i}+\overline{u'_k u'_i}\frac{\partial u_j}{\partial x_i}\right)$, $G_{jk}=-\rho\beta\left(g_j\overline{u'_k\theta}+g_k\overline{u'_j\theta}\right)$,

					$\phi_{jk} = \overline{p\left(\frac{\partial u_j'}{\partial x_k} + \frac{\partial u_k'}{\partial x_j}\right)}, \varepsilon_{jk} = 2\mu \frac{\partial u_j'}{\partial x_i} \frac{\partial u_k'}{\partial x_i}$
LES	(7) LES (Smagorinsky-Lilly)	1	0		
		u_j	μ	$-\frac{\partial \overline{p}}{\partial x_j} - \frac{\partial \tau_{ij}}{\partial x_j}$	$\tau_{ij} = \mu_t \left(\frac{\partial \overline{u}_i}{\partial \overline{x}_j} + \frac{\partial \overline{u}_j}{\partial \overline{x}_i}\right) + \frac{1}{3}\rho\tau_{kk}\delta_{ij}, \mu_t = \rho L_s^2 \sqrt{2\overline{S}_{ij}\overline{S}_{ij}}$

Table 2 Parameters at the jet nozzle of “high-Ri” and “low-Ri” cases

Case	Low-Ri	High-Ri
Jet velocity (mean) $U_0(m/s)$	1.88	0.24
Turbulent intensity $I = u/U_0$	6.0%	3.5%
Initial density difference $\Delta\rho_0/\rho_s$	0.5%	0.5%
Reynolds number $\mathrm{Re}_0 = \rho_s U_0 D/\mu$	24,000	3,200
Richardson number $Ri_0 = \Delta\rho_0 Dg/(\rho_s U_0^2)$	0.0002	0.01

Table 3 Mean squared errors of mean velocity self-similarity values

	MSE (Mean Squared Error)						
	Standard $k-\varepsilon$	RNG $k-\varepsilon$	Realizable $k-\varepsilon$	Standard $k-\omega$	SST $k-\omega$	RSM	LES
Low-Ri	1.86×10^{-3}	1.96×10^{-3}	1.99×10^{-3}	3.93×10^{-3}	6.10×10^{-4}	2.79×10^{-3}	2.45×10^{-3}
High-Ri	1.62×10^{-3}	7.39×10^{-3}	1.03×10^{-2}	8.18×10^{-3}	8.47×10^{-4}	1.15×10^{-2}	1.76×10^{-2}

Table 4 Mean squared errors of turbulent kinetic energy distributions

	MSE (Mean Squared Error)						
	Standard $k-\varepsilon$	RNG $k-\varepsilon$	Realizable $k-\varepsilon$	Standard $k-\omega$	SST $k-\omega$	RSM	LES
Low-Ri	6.26×10^{-7}	2.62×10^{-6}	4.26×10^{-7}	2.64×10^{-6}	3.94×10^{-7}	6.69×10^{-7}	8.39×10^{-7}
High-Ri	1.59×10^{-5}	4.64×10^{-6}	1.05×10^{-5}	1.17×10^{-5}	3.05×10^{-6}	5.82×10^{-6}	2.62×10^{-5}

Table 5 Mean squared errors of shear Reynolds stress distributions

	MSE (Mean Squared Error)						
	Standard $k-\varepsilon$	RNG $k-\varepsilon$	Realizable $k-\varepsilon$	Standard $k-\omega$	SST $k-\omega$	RSM	LES
Low-Ri	2.73×10^{-7}	1.25×10^{-7}	2.05×10^{-7}	6.19×10^{-7}	1.42×10^{-7}	1.94×10^{-7}	1.91×10^{-7}
High-Ri	1.34×10^{-6}	1.13×10^{-6}	1.52×10^{-6}	1.86×10^{-6}	7.01×10^{-7}	9.29×10^{-7}	1.21×10^{-6}

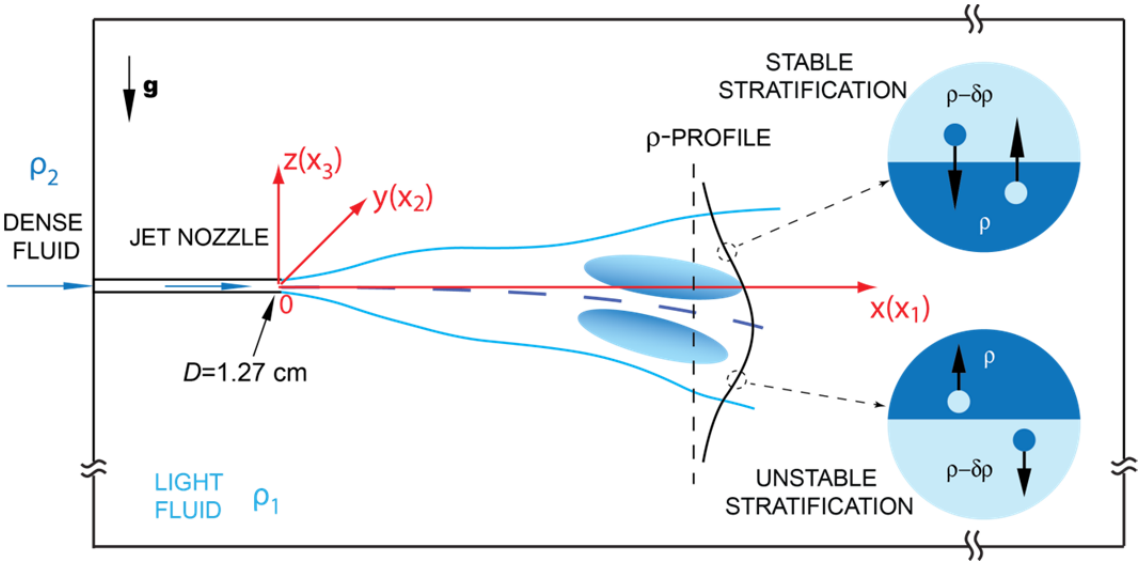

Figure 1 Setup of the stratified flow experiment (Xu and Chen 2012)

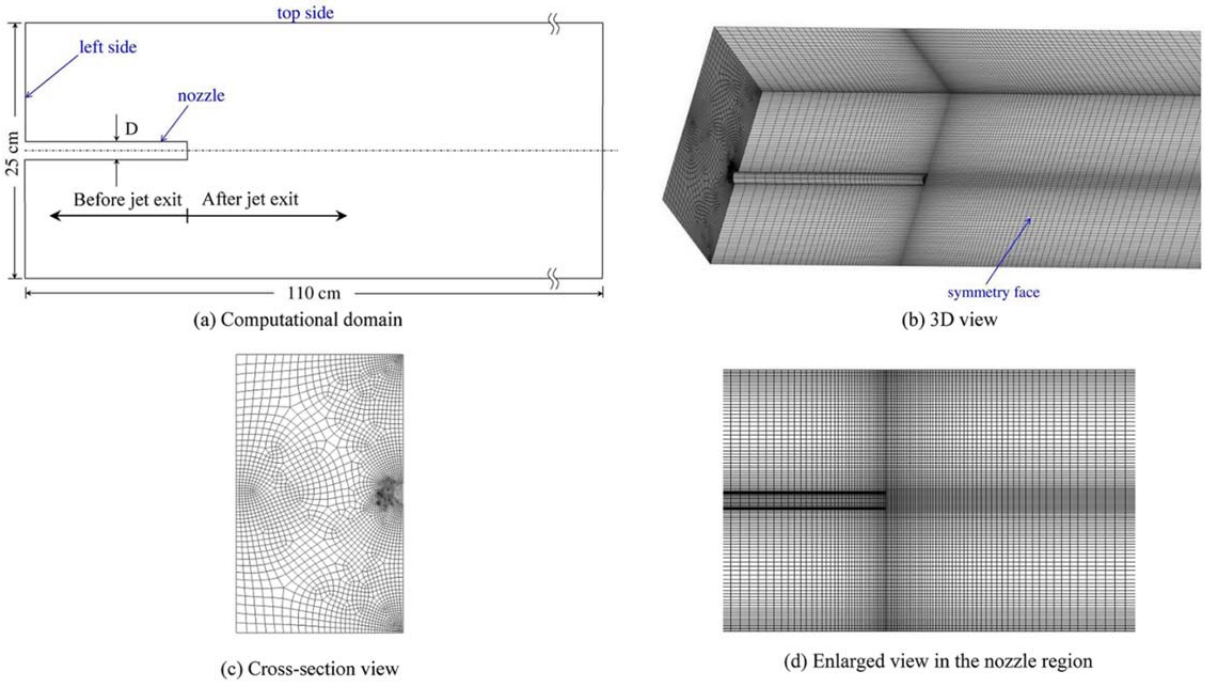

Figure 2 Computational domain and mesh structure in the present study

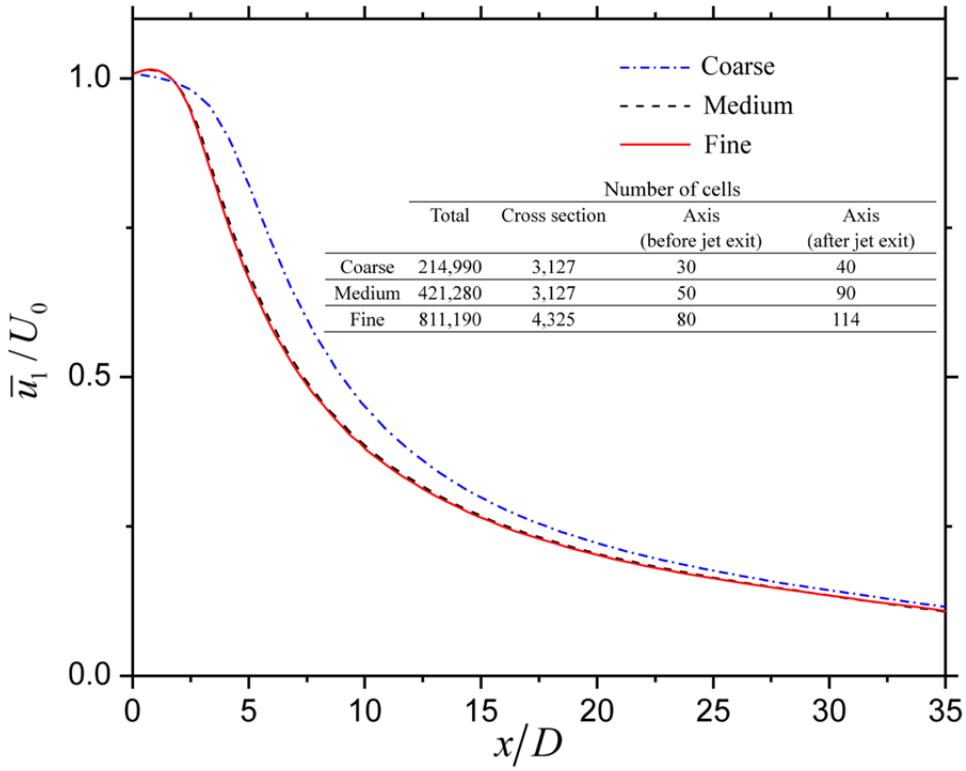

Figure 3 The jet centerline velocity predicted by RANS from different grids

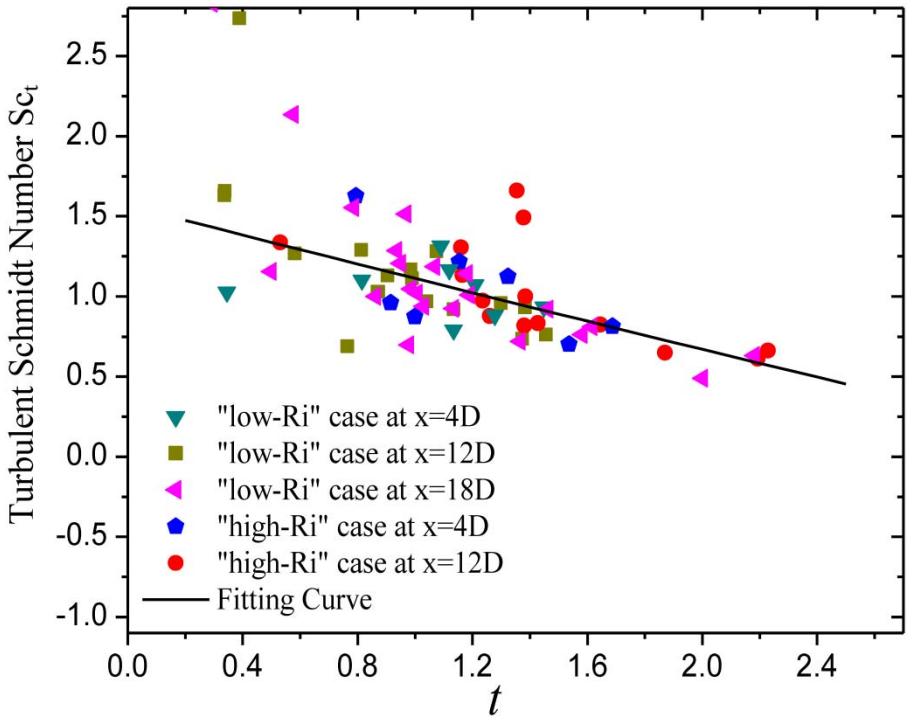

Figure 4 Fitting curve of expression (10)

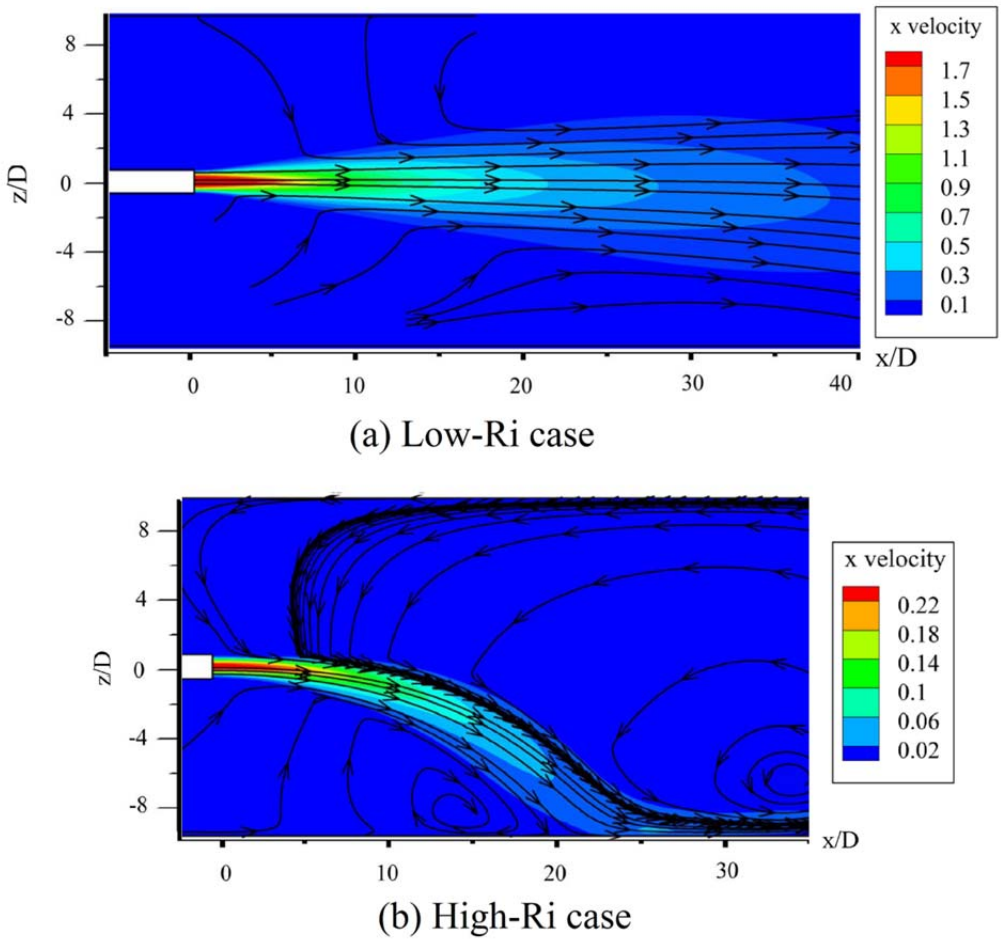

Figure 5 Velocity contours and streamlines from the simulation results (m/s)

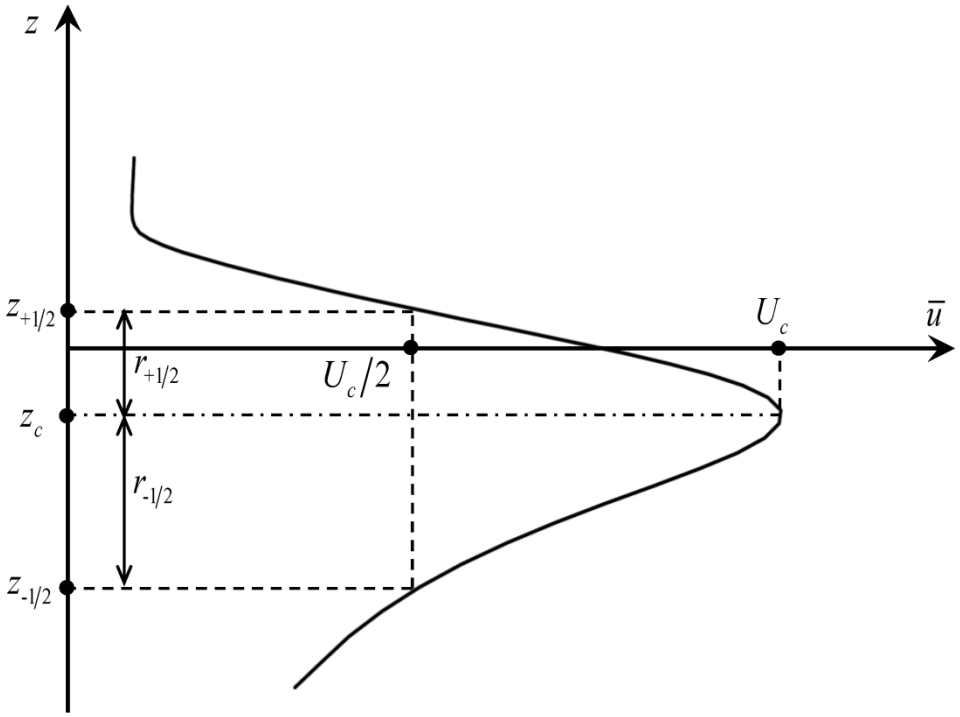

Figure 6 Mean velocity profile of a typical horizontal stratified jet

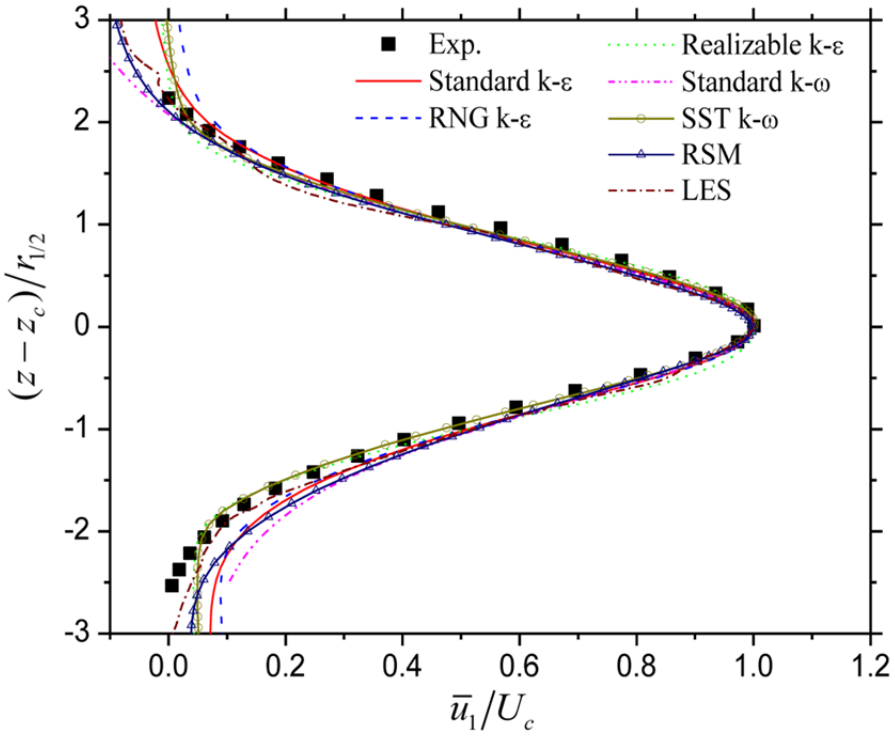

(a) Low-Ri case

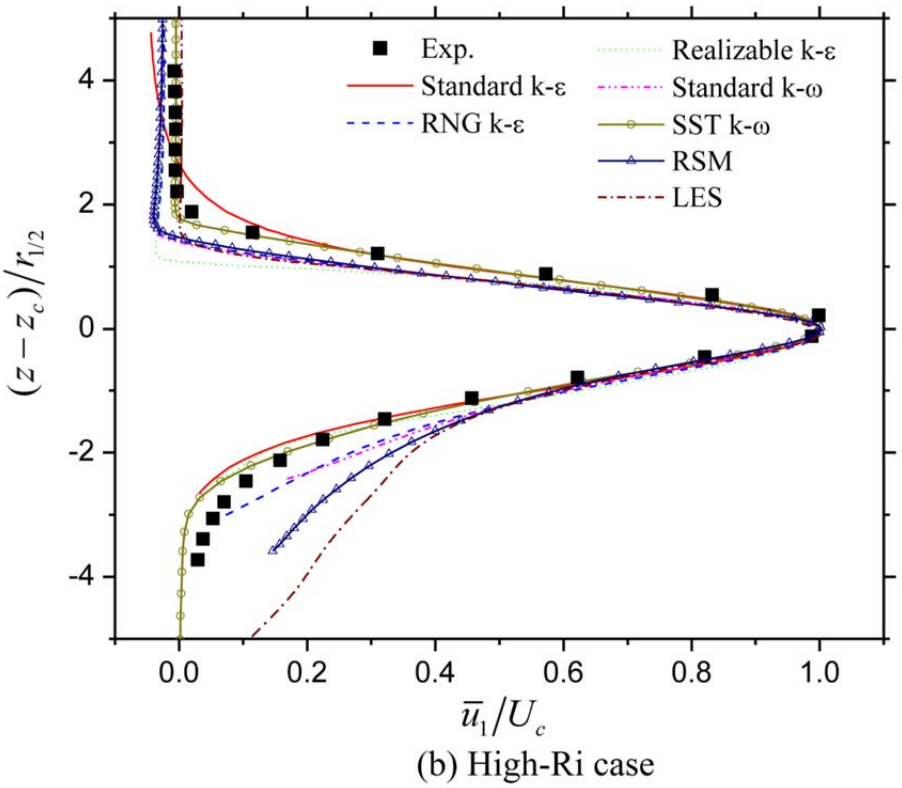

(b) High-Ri case

Figure 7 Self-similarity curves of mean velocity

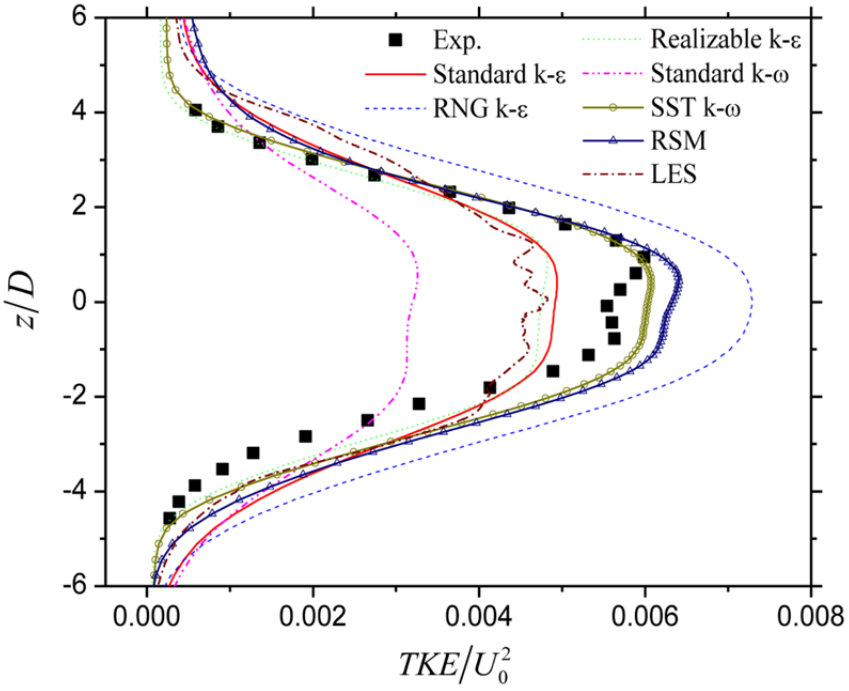

(a) Low-Ri case

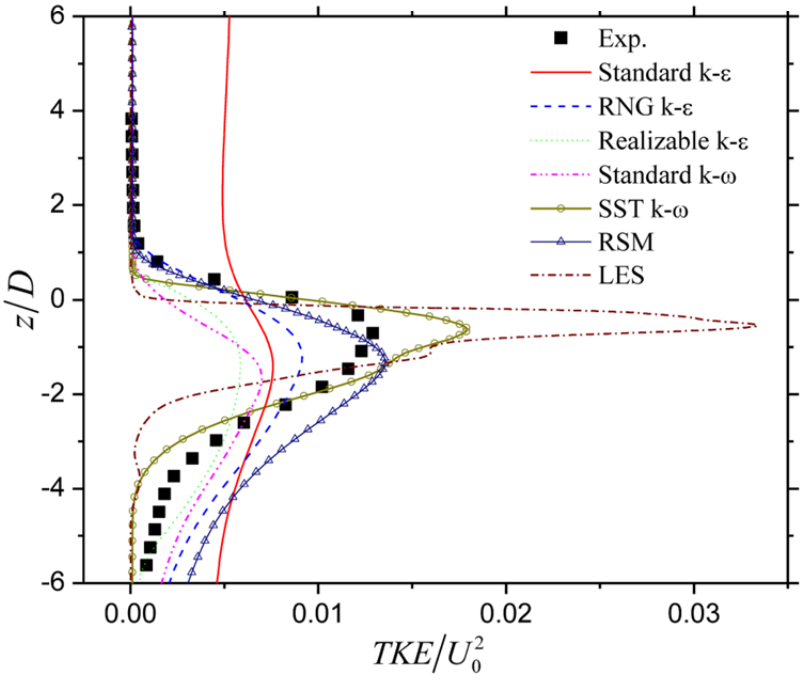

(b) High-Ri case

Figure 8 Turbulent kinetic energy distributions

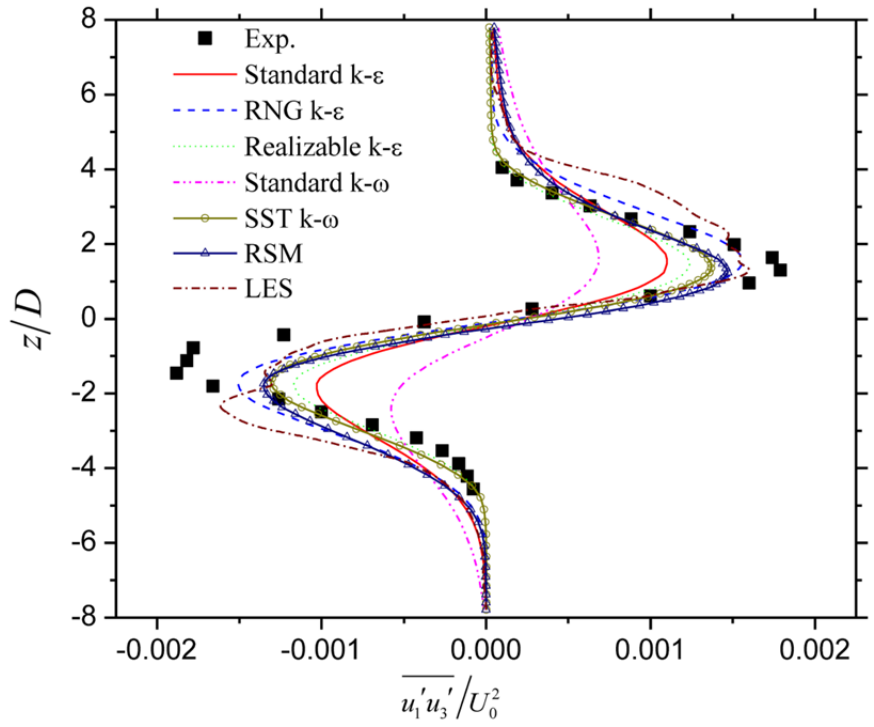

(a) Low-Ri case

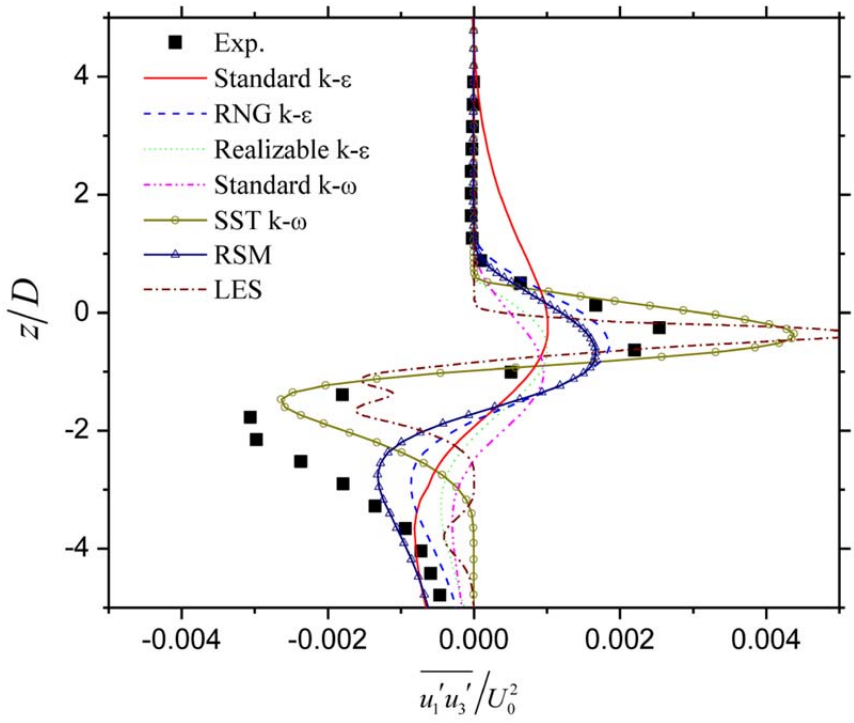

(b) High-Ri case

Figure 9 Shear Reynolds stress $\overline{u_1'u_3'}$ distributions

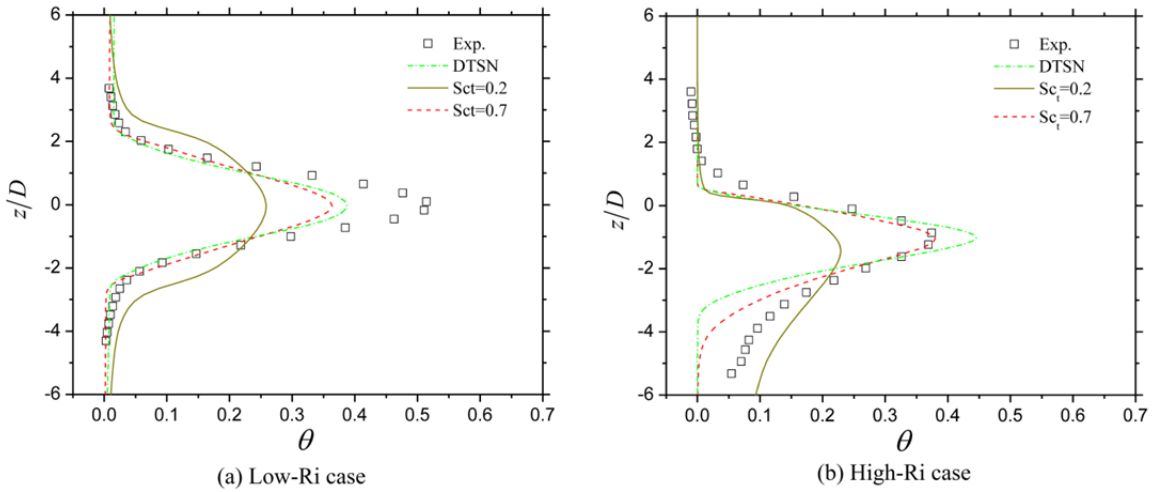

Figure 10 The normalized density distributions at upstream

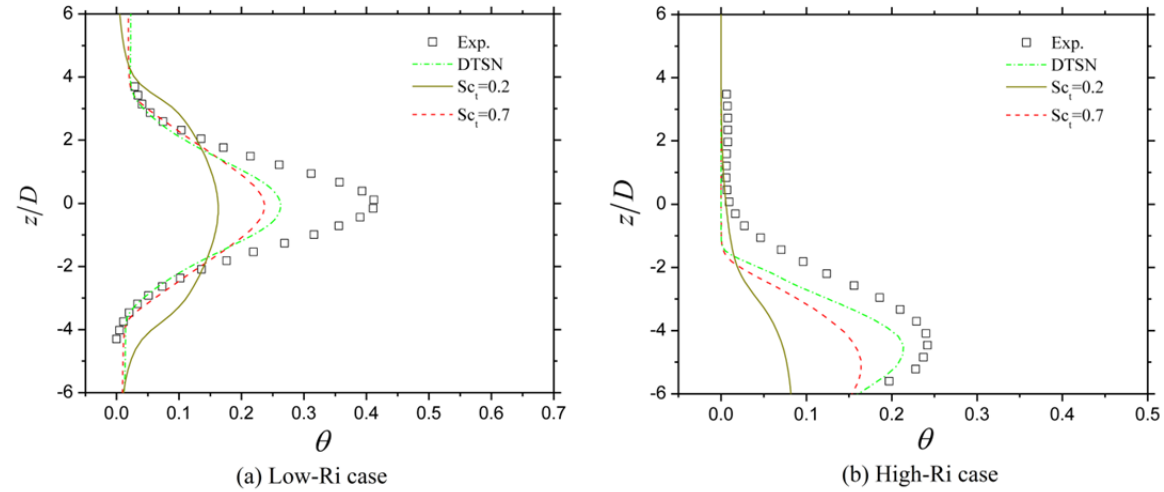

Figure 11 The normalized density distributions at downstream

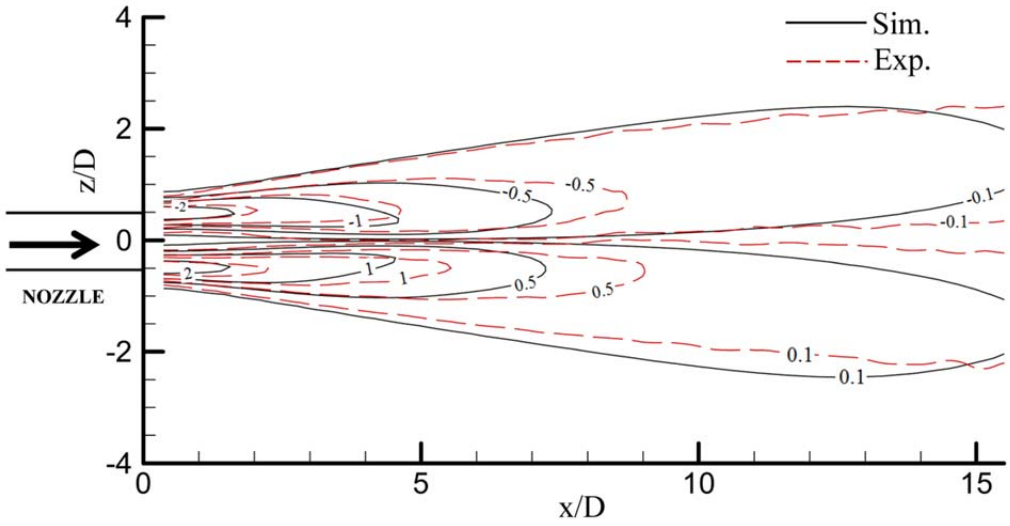

(a) Low-Ri case

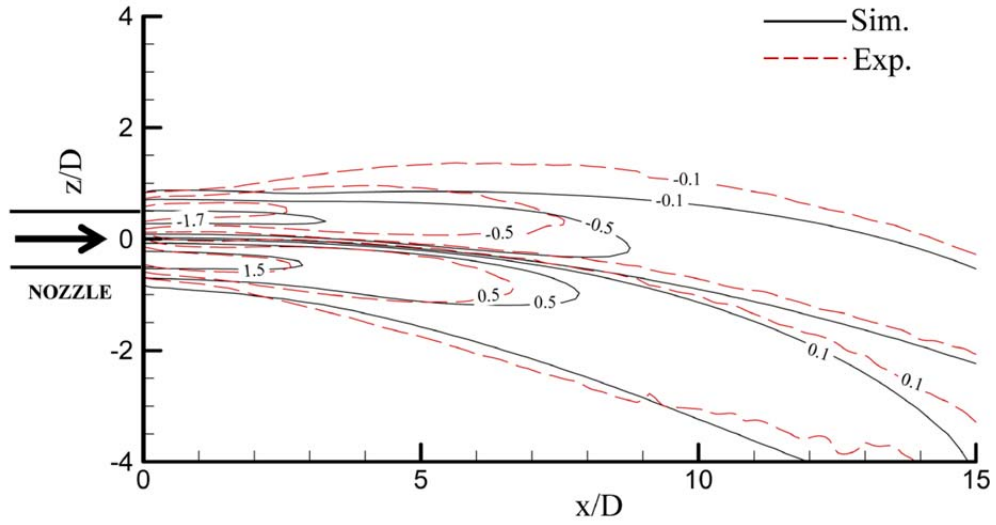

(b) High-Ri case

Figure 12 Vorticity (normalized as $\Omega_2 D/U_0$) contours in the low-Ri and high-Ri cases

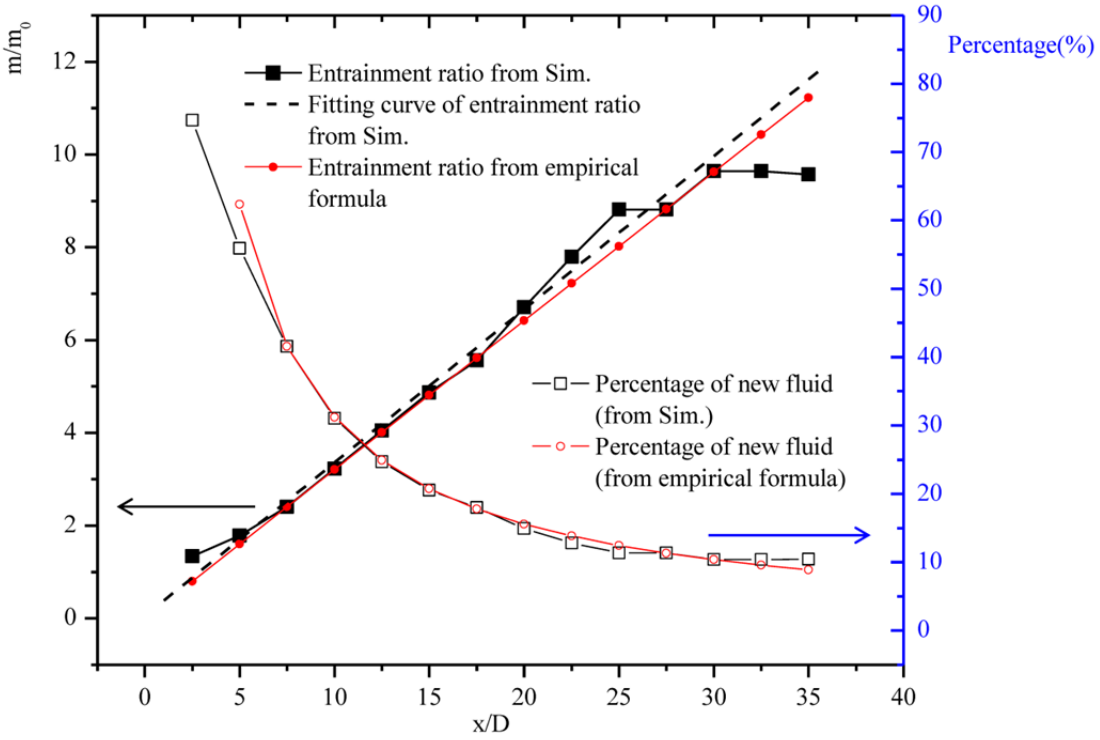

Figure 13 The entrainment ratio and the percentage of new fluid in the low-Ri case

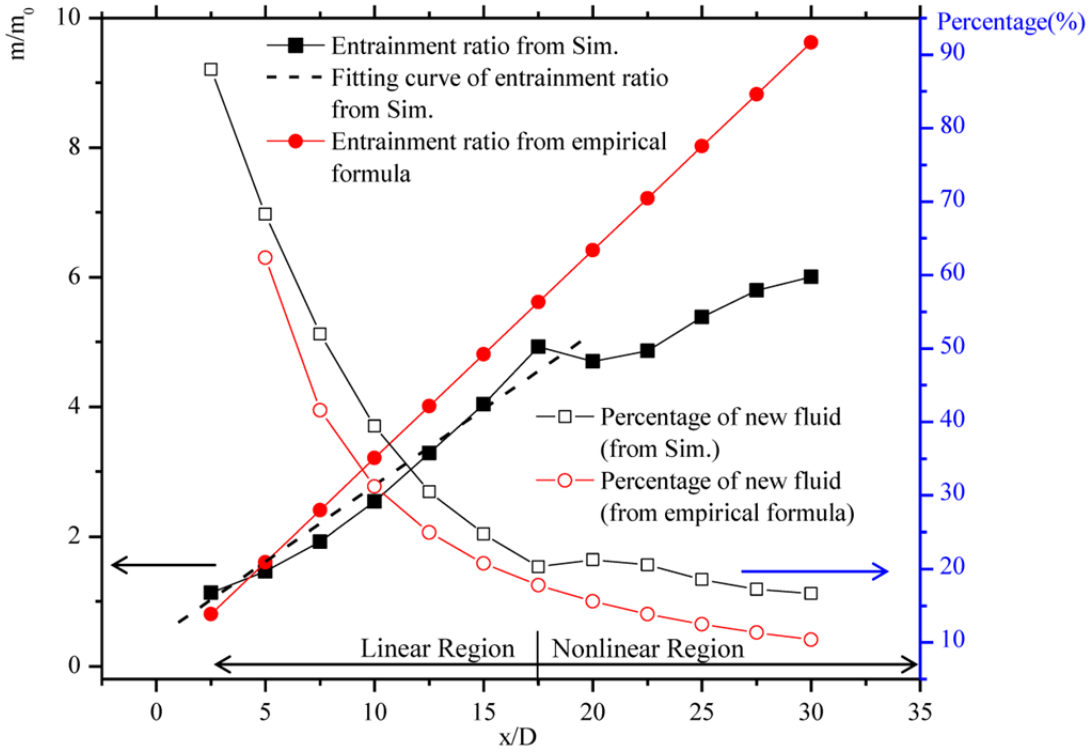

Figure 14 The entrainment ratio and the percentage of new fluid in the high-Ri case

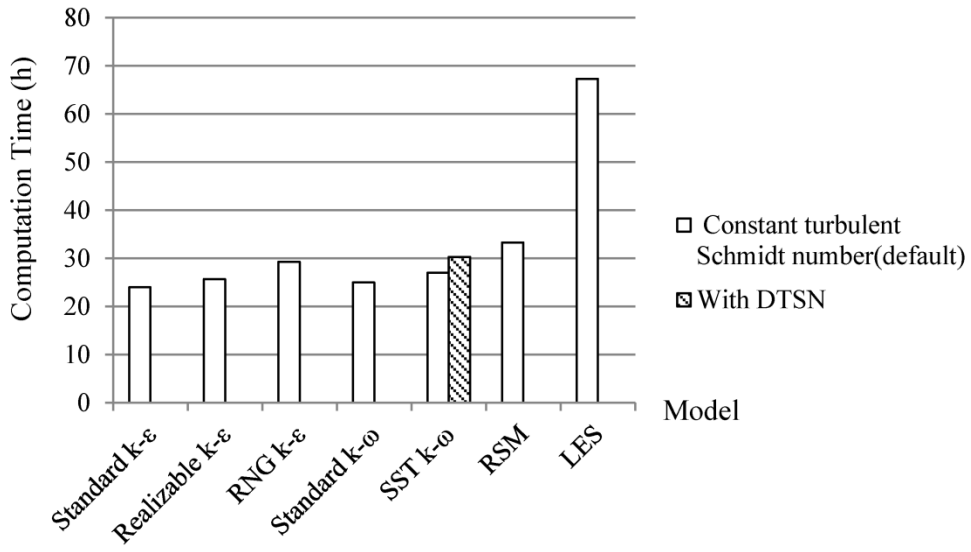

Figure 15 The computation time needed by different CFD models